From surface fault traces to a fault growth model: the Vogar fissure swarm of the Reykjanes Peninsula, Southwest Iceland

Thierry Villemin, Françoise Bergerat

From surface fault traces to a fault growth model: the Vogar Fissure Swarm of the Reykjanes Peninsula, Southwest Iceland.

Thierry Villemin[a], Françoise Bergerat[b] *

[a] EDYTEM (UMR 5204 CNRS-Université de Savoie), Campus scientifique, 73376 Le Bourget du lac Cedex, France - Thierry.Villemin@univ-savoie.fr

[b] ISTeP (UMR 7193 CNRS-UPMC), Université Pierre et Marie Curie, Case 117, 4, Place Jussieu, 75252 Paris Cedex 05, France - Francoise.bergerat@upmc.fr - Tel. 33 1 44 27 34 43

Keywords

Icelandic rift, Fissure swarm, Normal fault growth, Remote sensing, Photogrammetric techniques, Divergent plate boundary.

Abstract

The Vogar Fissure Swarm is one of four en-echelon fracture swarms that connect the Reykjanes Ridge to the South Iceland Seismic Zone and the Western Volcanic Zone. Occurring in an area of flat topography, this fissure swarm is clearly visible at the surface, where it can be seen to affect recent postglacial lavas. Using remote sensing methods to identify and measure all the faults and fractures in the swarm, combined with additional field observations and measurements, we measured 478 individual fractures, 33% of them being faults and 67% being fissures. The fracture lengths show roughly log-normal distributions. Most of the individual fractures belong to 68 main composite fractures, seven of which are longer than 2500 m and correspond to the main fault scarps of the fissure swarm. We showed that these main faults are distributed along five, equally spaced zones, ~500 m apart and a few kilometers long. We drawn 71 across-strike profiles to characterize the shape of the fault scarps, and 5 along-strike profiles to characterize the evolution of vertical throw along the main faults. Each fault consists of a coalescence of individual segments of approximately equal length. Fault throws are never larger than 10 m and are smallest at the junctions between individual segments. Analyses of along-strike throw profiles allowed us to determine the early stages of growth after coalescence. The earliest stage is characterized by an increase

in the throw of the central parts of segments. This is followed by a second stage during which the throw increases at the junctions between segments, progressively erasing these small-throw zones.

1. Introduction

Iceland's neovolcanic rift zone is the surface expression of the mid-Atlantic plate boundary. It consists of three main segments, known as the Northern, Eastern and Western Volcanic Zones, which are linked to the Kolbeinsey Ridge to the north and the Reykjanes Ridge to the south (Fig. 1A). Southern Iceland's Reykjanes Peninsula lies between the Western Volcanic Zone and the offshore Reykjanes Ridge, and includes features characteristic of both divergent and transform-type plate boundaries. The general purpose of the present research is to better understand fault growth at such divergent plate boundary. The Vogar fissure swarm provides the most suitable conditions for this, as the structures are clear on postglacial lava flows and not on loose terrain with vegetation.

The volcanic zones are crossed by what are generally referred to as fissure swarms (Sæmundsson, 1978) and include central volcanoes, eruptive volcanic fissures, tension fractures, and faults. Numerous studies have examined the fracture geometry of some of Iceland's fissure swarms (Sæmundsson 1978, 1992; Guðmundsson, 1987b; Opheim and Guðmundsson, 1989; Guðmundsson and Bäckström, 2000; Tentler and Mazzoli, 2005; Friese, 2008; Hjartardottir et al., 2009), and the main features of the Vogar Fissure Swarm have been described as part of general studies of the Reykjanes Peninsula (Guðmundsson, 1980, 1986, 1987a; Grant and Kattenhorn, 2004; Clifton and Kattenhorn, 2006). Other research has shown that detailed topographical analyses of fissure swarms can be used to determine the geometry and mechanical behavior of the underlying extensional structure (Guðmundsson, 1992; Angelier et al. 1997; Dauteuil et al., 2001, Acocella et al., 2003).

Investigations of the spatial distribution of faults and fissures are essential for understanding the mechanisms underlying fault growth, and, more generally, brittle failure behaviors (Cowie et al., 1996; Torabi and Berg, 2011). Linkage and forward propagation models can be used to explain field observations. How fault segments coalesce and how this coalescence produces changes in fault architecture have been particularly well documented in different rock types and in different tectonic settings. Numerous studies have analyzed either surface (horizontal) faulting configurations (e.g., Peacock, 1991; Cartwright et al., 1995; Childs et al., 1995; Huggins et al., 1995) or vertical faulting configurations (e.g., Peacock and Zhang, 1993; Childs et al., 1996; Mansfield and Cartwright, 1996; Schöpfer et al., 2006). In fact, linkages between the different parts of normal faults occur both vertically and horizontally, and on a broad range of scales. Despite all these studies, some aspects of fault initiation and development are still poorly understood and subject to debate.

The aims of the present work were thus: (1) to produce a detailed description of the structure of the Vogar Fissure Swarm (Fig. 1C) as the basis for an analysis of its fracture style and behavior, and (2) to draw up a 3D tectonic model for the formation and growth of normal faulting in this type of fissure swarm characteristic of the Icelandic divergent boundary. To do this we combined (i) remote mapping based on geo-referencing, orthorectification, and 3D photogrammetric restitution of aerial photographs with (ii) geodetic (GPS) ground control points and (iii) field observations and measurements taken to check the remote data. The resulting accurate map of the Vogar Fissure Swarm allowed us to analyze the layout and throws of the normal faults in three dimensions and at a level of detail not previously attained for this size area. We (i) determined the type, length, and spacing of 478 individual decameter- to kilometer-scale fractures, (ii) characterized the shape of the fault scarps in 71 across-strike profiles, and (iii) measured the along-strike evolution of vertical throw along five main fault scarps.

2. Geological setting

The deformation in southwest Iceland is accommodated by three major structures: the Reykjanes Peninsula (RP) to the south, the Western Volcanic Zone (WVZ) to the north and the South Iceland Seismic Zone (SISZ) to the east (Fig. 1A). The direction of plate motion at the 30°-trending Reykjanes Ridge (offshore segment of the Mid-Atlantic Ridge) to the south of Iceland is N104° (DeMets, 1990, 1994). To the east, the SISZ is a major E-W left-lateral transform zone that connects the RP to the Eastern Volcanic Zone (EVZ). However, part of the extension continues along the WVZ. The RP is highly oblique to the direction of plate motion and geodetic studies have shown that plate spreading is accommodated both by left lateral shear (17-19 mm/yr) and by opening (7-9 mm/yr) below a locking depth of 6-9 km (Árnadóttir et al., 2008; Keiding et al., 2009). Leveling measurements along profiles through the RP indicate vertical displacement on normal faults of up to several millimeters over a period of about ten years, together with regional tilting (Tryggvason, 1974, 1982).

The divergent plate boundary in the RP runs for 70 km between Hengill volcano to the north and the tip of the peninsula to the south, and has an overall trend of ~70°. It consists of four main en-echelon fissure swarms, trending ~45°. From west to east, these swarms are the Reykjanes, Krýsuvík, Bláfjöll, and Hengill swarms (Fig. 1B).

The Reykjanes Fissure Swarm is a 35 km by 5-8 km zone of recent faulting, fissuring and volcanism that is directly connected to the offshore Reykjanes Ridge to the south. Onshore, it extends from the northern coast of the RP to its southwestern tip (Fig. 1C), cutting through postglacial basaltic pahoehoe lavas older than AD 871 and younger than 0.8 My. Its northern part, called the Vogar Fissure Swarm (VFS), is separated from its southern part by aa lavas younger than AD 871 (Jóhannesson and Sæmundsson, 2009).

The VFS (Fig. 1C) clearly shows the recent fracture pattern, allowing it to be geometrically analyzed over a wide range of scales, from minor fissures to large fault-tilted blocks.

3. Methodology

We used 1:25,000 scale aerial photographs obtained from "Landmælingar Íslands" (Geographic Survey of Iceland) to map the fractures of the VFS and analyze their number, length, density, and throws. These photos, which covered an area of approximately 30 km^2, were digitized at a resolution of 1200 dpi (i.e. a ground resolution of 0.5 m). The main data acquisition stages involved building a mosaic of aerial photographs and carrying out stereoscopic analyses of photographic pairs. Additional detailed observations and measurements were made using photographs taken from a helicopter.

We used ErMapper® software to spatially register and rectify the photographs with respect to Ground Control Points (GCP) and to a Digital Elevation Model (DEM) of the area at a resolution of one point every 90 m. GCP coordinates were measured using GPS mono-frequency Trimble receivers and GPS data were analyzed using Pathfinder Office® software. Mean calculated errors were 2-5 cm (horizontal) and 5-10 cm (vertical), so measurement uncertainties were negligible compared with the measurement errors the irregular texture of the lava flows would induce in ordinary field observations. Following orthorectification of each photograph, we created a mosaic for the whole study area (Fig. 2), which we then used as a base map for plotting the fracture traces, added using Autocad Map®.

Stereo-photographic pairs were constructed in line with the principles of parallel stereoscopy (Kasser and Egels, 2001) and using the Poivilliers software developed by Yves Egels at France's National Geographic Institute. Overlaps between two adjacent photographs were ~60%. The process involved two main steps: (i) creation of photogrammetric models and (ii) use of these models to characterize the types of fracture and to measure scarp heights, which can be considered to represent the vertical throws of the faults, as erosion is negligible in Holocene lava flows.

Each stereo pair was constructed using interior and absolute (exterior) orientation parameters. When constructing stereo pairs in this way, interior orientation requires that camera fiducial marks are positioned independently for each photograph, so the location of the principal point (projection of the perspective center on the image plane) can be calculated. We then identified several tie points and GCPs on both photographs of a stereo pair in order to simultaneously obtain relative and absolute orientations. Each point was identified by its coordinates on both the left (xl, yl) and right (xr, yr) images. This step is based on co-linearity and straight-line co-planarity conditions (Kasser and Egels, 2001). At least three GCPs spread across the entire stereo pair and at least five tie points are needed to determine absolute orientations. We used ground coordinates from GPS benchmarks as GCPs. The accuracy of our photogrammetric models enabled us to determine 3D coordinates for each point with horizontal and vertical precisions of 0.5 m. The lava flows have such uneven surfaces that altitude differences of less than 0.5 m are not significant (Guðmundsson, 1992).

This process allowed us to identify and position each fracture in three dimensions, and to plot the fractures on the mosaic, using different colors to depict throw and opening characteristics (Fig. 2). The resulting fracture map was used to analyze the geometry of individual fracture traces within the VFS. We did not do any mapping in the Skógfellahraun aa lava flow (Fig. 2) because of the difficulty of following (and measuring) fracture traces in these very friable and jumbled lavas.

We used the stereo pairs to draw along-strike topographic profiles of the footwalls and hanging walls of five main fracture lines over a distance of 14 km. We obtained 20 topographic profiles by drawing four profiles for each fracture line, two on the hanging wall and two on the footwall, at distances of 20 m and 40 m from the main scarp. We then used these topographic profiles, interpolating where necessary to obtain the points needed for calculating differences in elevation between the hanging wall and the footwall for each fracture line (see Fig. 10, section 4.6).

Moreover, punctual field observations and measurements have been carried out as control points to validate the mapping of fractures and the profile values.

4. Results

The following descriptions of the geometrical characteristics of the fracturing are based on data obtained by analyzing aerial photographs as described above, combined with field observations and measurements.

4.1 Fracture type terminology

We produced maps of the VFS by tracing features from stereoscopic aerial photographs. The term "fracture" is used hereafter to refer to all types of mechanical discontinuity with a tectonic origin. We differentiated two types of fracture, those with vertical throw, referred to as normal faults, and those without vertical throw (or with vertical throw smaller than 0.5 m which corresponds to the accuracy obtained by the photogrammetric model), referred to as fissures. Some normal faults were open, others were not (Fig. 6). The normal faults in the VFS are actually vertical faults with both vertical displacement and dilation (Fig. 5). The Icelandic names for the main fault scarps, which also have a significant dilation component, end in "gjá" (Fig. 2), which means gap. These faults become true normal faults (shear) at depth (e.g., Angelier et al., 1997).

We refer to fractures that can be traced continuously as "individual fractures". Individual fractures commonly concentrate in fracture strips that may be discontinuous and are of varying lengths. Most fracture strips, which we refer to as "main composite fractures" (Fig. 3), are composed of several aligned individual fractures, generally including both fissures and faults (Fig. 2). For mapping purposes, we considered parallel main composite fractures to be separate if they are more than 125 m apart and aligned main composite fractures to be separate if they are more than 250 m apart.

One difficulty with this type of mapping is the difference between the scale of the photographs and the scale of the map. At the scale of the photographs used for our study, two small lines close together may be indistinguishable and appear as a single line, whereas they would appear as two separate lines on a more detailed photograph or in the field. In addition, some large fracture lines may be quite thick due to the coalescence of several individual but indistinguishable fractures.

4.2 Number of fractures and organization of the network

We mapped 478 individual fractures (a few were only partially mapped because of the presence of the aa lava flow) in the study area (Fig. 2), 33% of which are normal faults and 67% are fissures. Most belong to the 68 main composite fractures (Fig. 3), seven of which are more than 2500 m long and correspond to the main fault scarps of the fissure swarm (Fig. 4).

Except close to the Skógfellahraun aa lava flow, the main composite fractures in the western part of the VFS are composed mostly of fissures, whereas those in its eastern part are composed mostly of normal faults. The VFS is ~10 km long, measured from the aa lava flow to its northeastern tip, and tapers from ~4.5 km wide close to the aa lava flow to ~3 km wide at its northeastern tip.

The western edge of the VFS is formed by a major, east-facing normal fault, called Hrafnagjá (Fig. 2; R16 in Fig. 3), whereas its eastern edge is formed by a series of open fissures, called Brunnastaðaselsgjá (Fig. 2; R66-67 in Fig. 3). The area between these two boundaries contains five major west-facing normal faults in a step pattern (Fig. 2). The easternmost major normal fault scarp is called Grindavikurgjá (Fig. 2; R59 in Fig. 3). Individual fracture strikes (fissures and faults), based on their mean linear orientation weighted by the length of each fracture segment, are between N30°E and N70°E, with a mean strike of N55-60°E (Fig. 3).

4.3 Length and density

The main composite fractures are between 250 m and 5.6 km long (Fig. 7 C). Individual faults are between 34 and 1288 m long (mean length 229 m). Individual fissures have a comparable minimum length (23 m) but maximum and average lengths are significantly shorter (545 m and 139 m, respectively). Because the aa lava flows (southwestern part of Fig. 2) prevented us fully mapping a crucial part of the faults, their mean and maximum lengths were almost certainly underestimated. This is only a minor problem for the fissuring. However, some of the shortest fissures (<10 m) are probably masked by soil and grass, so this class is likely to be under-represented. What is more, these small fissures are similar in size to non-tectonic, cooling fractures in the lavas, so it was not always possible to measure them.

The length distributions of all the sets of fractures (Fig. 7 A and B) show roughly log-normal distributions ("heavy tail" type); therefore, the average length is not characteristic. Consequently, the classes with the highest frequencies are [75-100 m] for the faults and [50-100 m] for the fissures.

The cumulative lengths of all the fractures mapped were 44.9 km for the fissures and 35.7 km for the faults, which gives fracture densities for the area affected by faulting of 1.45 m/m^2 and 1.15 m/m^2, respectively.

4.4 Spacing

We measured the spacing between the fractures in the VFS along profiles perpendicular to the maximum frequency directions indicated by the rose diagrams (Fig. 3). Profile lengths (distance between most northwesterly and most southeasterly fractures) were between 1700 m and 4100 m. The linear density of fractures (number of fractures per unit length) depends on the type of fracture:

- The density of the fissures is extremely variable, depending on where the cross-section was taken. The spacing distribution shows modes at 75 m, 225 m, and 450 m (Fig. 8). There are probably modes at other multiples but these modes are difficult to determine due to the limited number of sampling values. These multiples result from the non-persistence of the fissures.

- The spacing distribution for all the individual fractures (faults and fissures) also shows modes at 75 m, 225 m, and 450 m (Fig. 8). Some multiples may be less visible because fractures do not necessarily extend across the entire study area. Fissures linking two segments of a fault, thereby making the combined fissure longer, are very common.

- The spacing distribution of the composite fractures shows only two modes, at 225 m and 450 m (Fig. 8). The mode at 75 m is not present because fractures that are less than 125 m apart were shown by a single line when we drew the composite fractures map.

The three modes noted above can be seen clearly in Figures 2 and 3. Their significance is discussed in section 5.

4.5 Topography of the fissure swarm and across-strike throws

Using the automatic protocol described in section 3, we drew 71 across-strike profiles through the entire fissure swarm (numbered 0-70 in Fig. 3). Figure 9 shows ten characteristic profiles. We calculated elevations every meter along each profile. Outliers were removed from the raw results according to two criteria. First, we removed outliers for which the value of the local correlation parameter between the two images for each point was less than 0.5. Second, we used a moving average filter on the nearest 24 points to remove elevations that differed by more than 5 m. Even after this filtering, the elevation signal was still quite noisy.

As the amplitude of the noise was around 1 m, some normal faults with vertical throws of less than 2 m may not have been distinguishable from the background noise. Taking into account the uncertainties of the calculation method, we obtained a mean throw of 8-10 m for the main faults (Fig. 9).

In the south of the network, the profiles clearly show that the lava flows dip gently (~3%) to the NW. This surface dip decreases progressively towards the north of the network.

Many faults display an obvious bulge on the surface of the lavas on the upthrown side ~50 m from the fault scarp (e.g., R16 in Fig. 9 and detail in Fig. 9A and 9B).

In the south (sections 0-40, Fig. 3), the entire fissure swarm has a graben structure, bounded to the northwest by the east-facing Hrafnagjá normal fault (R16). In places, this large fault is associated with a secondary normal fault (e.g., R21 on profile 23, Fig. 9). To the southeast, the graben is bounded by the west-facing Grindavikurgjá normal fault (R59. This fault is not shown on the across-strike profiles because of correlation difficulties during the automatic plotting due to the location of this fault on the edge of the photographs). Faulting deformation between the two boundary faults is mainly accommodated by west-dipping normal faults, especially R24, R28, R38 and R55 in the southern part of the fissure swarm (Fig. 9). These sub-parallel normal fault scarps form a step pattern that is characteristic of the southern part of the VFS (see also Fig. 4).

The pattern in the northern part of the VFS is slightly different, as there is no equivalent of the Hrafnagjá fault, and the western part of the network is composed mostly of fissures and minor faults. Consequently, the general structure changes to a hemi-graben, bounded to the southeast by two major normal faults (Klefgjá and Grindavikurgjá, R48 and R59, Fig. 9)

Some scarps along a single fault vary in shape. Generally, faults at the surface of the VFS are characterized by a near-vertical fault plane (e.g., R16 A in Fig. 9, and Fig. 5) but in some places the fault plane is flanked by a narrow monocline that, on the scale of our across-strike profiles, appears as a smooth bulge (e.g., compare R28 D and C in Fig. 9; see also Grant and Kattenhorn, 2004).

In this study, we decided not to focus on fault width (opening) for two reasons. (i) The methodology we used did not allow us to measure small widths, thereby precluding an exhaustive analysis. (ii) The true width is often less than the measured width due to the existence of graben-like structures. Despite the uncertainties caused by this overestimation of some of the widths, Guðmundsson (1987a) produced some accurate width measurements in the VFS (1076 points measured) along six main fractures (R16, R24, R28, R38, R55 and R67 in the present study). He obtained a mean width for all the points measured of 0.6 m and an absolute maximum width for a single fracture of 7.5 m.

4.6 Changes in along-strike fault throws for the main composite fractures

We also produced automatic plots of along-strike profiles (see section 3) for five main composite fractures: the east-facing fracture (R16) that forms the western boundary of the VFS and four west-facing fractures (R24, R28, R38 and R48) within the fissure swarm (see Fig. 3 for locations). For each main composite fracture, we started with the central trace (axis of the fractured strip) and calculated two sets of two parallel traces, 20 m and 40 m from the main scarp, on the hanging wall and on the footwall, respectively. The mean distance between points was ~5 m. We then used the automatic image correlator to calculate the elevation of each point on all the traces.

Each of the four profiles for a given fracture has the same number of points. The four points with the same index on each profile represent a cross-section of the fracture and the differences in their elevations correspond to the vertical throw at distances of 20 m and 40 m from the main scarp. The profiles in Figure 10 show along-strike variations in these differences, that is, changes in the vertical throw.

Main composite fracture R16 (Hrafnagjá) is fully visible over a distance of 2500 m. The profiles show that the throw is greatest in the central part of the fault and decreases towards its tips. This fault forms the western boundary of the VFS. Its maximum throw is ~10 m.

The other four normal main composite fractures we analyzed are located between the two main boundary faults and are all west facing. They range in length from 2800 m to 5400 m, but the Skógfellahraun aa lava flow covers the southwestern ends of three of these fractures (R24, R28, R38).

Main composite fracture R48 (Kvelfgjá) is 5400 m long and is visible in its entirety. Its profile consists of three similar, 1500-2000 m long segments, each of which is similar in size and shape to fault R16. Each segment has a mean maximum throw of 8-10 m in its central part. This throw decreases to zero at the segment tips. A second periodicity, with an amplitude of 2-4 m, modulates the profile of each segment every 250-500 m.

Main composite fracture R38 is visible over a distance of ~2800 m. It has a maximum throw of 11.5 m and the throw decreases towards the northeast. The throw decreases ~1000 m from the trace, corresponding to the junction with another main composite fracture (R36 in Fig. 3 and Fig. 11). To the southeast, fractures R36 and R38 are parallel to each other and each fracture probably accommodates part of the deformation.

Main composite fracture R28 is 3500 m long and has a maximum throw of ~10 m. As for main composite fracture R48, the profile is modulated by a ~500-m periodicity with an amplitude of ~5 m. The throw decreases in four places along the profile where the fracture is mostly composed of fissures, rather than normal faults.

Main composite fracture R24 is 3000 m long. Again, it has a maximum throw of ~10 m but there is no variation in the throw along a significant part of the profile. Then, the throw decreases steadily to the northwest over the last 500 m.

Compared with the throw profiles for complete fractures R16 and R48, it is evident that the southeastward decrease in throw is missing from main composite fractures R24, R28 and R38. This decrease probably occurs in the part of the fractures in the aa lava flow. The total length of these faults could not be measured.

In general, the throws calculated from the profiles 20-m and 40-m from the main scarp have very similar shapes along the main composite fractures. The 20-m and 40-m throw profiles for R28 and R38 are almost identical. The forms of the 20-m and 40-m profiles for R48 are very similar, even in their minor variations (small peaks and troughs). The only difference is the throw itself, as the throw 40 m from the main scarp is systematically smaller (by 2-3 m on average) than the throw 20 m from the main scarp. The differences in the R16 and R24 profiles are greater, not only because the 40 m profile (for R24) has a systematically smaller throw, but also because there are discrepancies between peaks and troughs (1.5 km and 2 km from the southwestern tip for R16, and 0.5 km and 1.3 km from the southwestern tip for R24). The differences between the 20-m and 40-m profiles are mainly due to the lava flow almost systematically sticking up slightly on the upthrown side close to the fault scarp (Fig. 9). Local discrepancies, such as those shown by profiles R16 and R24, are due to the presence of lava swells of volcanic origin.

4.7 The linkage zones

The main composite faults are composed of alignments of several individual fractures, presenting different types of linkage at the surface. There are two main types of linkage pattern: (i) a non-overlapping pattern with aligned or non-aligned segments, and (ii) an overlapping pattern with fault segments that curve at their tips. The linkage of smaller segments into larger segments allows the growing of faults and depend in detail of the distances between their nearby tips relative to the segment lengths (Guðmundsson, 2011).

Although some neighboring aligned segments tend to propagate toward each other (Fig. 12a) and a number of non-aligned segments are linked by en echelon or oblique fractures that develop between fracture tips (Fig. 12b), most linkages form overlap patterns. We noted three types of overlap feature. In some overlapping segments, the tips of one segment propagate to the sidewall of another segment along a curved path (Fig. 12c). In other overlapping segments, parallel en-echelon fractures develop in the linkage zone (Fig. 12f). The final type consists of parallel fault segments that overlap over a long distance (Fig. 12e). Some linkage zones are complex and can include, for example, oblique and parallel fractures (Fig. 12g) or a horsetail feature (Fig. 12d, h).

In general, linkage zones connect the hanging wall of one fault to the footwall of another fault and transfer the displacement from one fault to the other. For both overlapping and non-overlapping pattterns, open fractures can develop in the linkage zone (Fig. 2, Fig. 12). Similar intermediate (or mixed) patterns to the ones we found in the VFS have also been described in other Icelandic fissure swarms (Guðmundsson, 1987a, b; Acocella et al., 2000; Grant and Kattenhorn, 2004; Tentler, 2005; Tentler and Mazzoli, 2005; Friese, 2008).

Topologically, junctions between fracture traces can be described as immature and mature. In the immature state, it is possible to pass from one side of a fracture to the other without crossing any visible fissure or fault. In the mature state, the two main segments are completely connected and the two sides of the fault are totally separated; hence, fragmentation is complete (Fig 13). Immature junctions are quite frequent along the main composite fractures of the VFS.

5. Discussion: formation and growth of fissures and normal faults

In the VFS, the spatial distribution of faults and fissures, as well as the changes in fault throws, allow investigating linkage and forward propagation models both vertically and horizontally. They permit to highlight the process of fault segments coalescence and the resulting changes in fault architecture.

5.1 Surface deformation and structure at depth

In the Icelandic crust, magma intrusion at depth is generally agreed to have a major effect on the development of tectonic structures (e.g., Angelier et al., 1997). However, how normal faults grow vertically is an important unanswered question. Evidence provided by combining seismicity and magma accumulation data suggests that most normal faulting occurs at depths of 1-5 km (Einarsson, 1991; Hreinsdóttir et al., 2001). A number of models favor upward propagation from depth (Grant and Kattenhorn, 2004; Tentler, 2005), whereas others promote downward propagation from the surface (Acocella et al., 2003). Others still advocate sub-simultaneous downward and upward propagation (Guðmundsson, 1992; Martel and Langley, 2006).

It has often been assumed that a single shear zone will usually be unable to grow in its own plane and develop into a normal fault (e.g., Scholz, 2002). Guðmundsson (1992) suggested two mechanisms for normal fault initiation: (i) nucleation from large-scale tension fractures originating at the surface and propagating to significant crustal depths, and (ii) nucleation on sets of en-echelon joints when lava flows become tilted. Guðmundsson maintains that these two mechanisms can occur concurrently, with the upper part of a fault nucleating on a large-scale tension fracture and the lower part nucleating on a set of inclined joints. He also suggests that large-scale tension fractures change into normal faults when they reach a critical depth that partly depends on the tensile strength of the host rock. Thus, a mean tensile strength of 3 MPa (Haimson and Rummel, 1982) corresponds to a change at a crustal depth of ~0.5 km. The critical crustal depth at which inclined joints start to link up into normal faults, taking into account the associated friction, is ~0.8 km, and the process is common at ~1.5 km (Guðmundsson, 1992). Given these two nucleation zones, Guðmundsson concludes that normal faulting starts to nucleate at crustal depths of 0.5-1.5 km.

Following studies of the Krafla fissure swarm in northeast Iceland, Angelier et al. (1997) and Dauteuil et al. (2001) put forward a comparable model to Guðmundsson's for the relationships between open fracture geometry observed at the surface and normal fault dip inferred at depth. In this model, normal shear also plays a major role at intermediate depths in the upper brittle crust and normal faulting occurs along planes with a mean dip of 60-75° at a crustal depth of ~1 km. No hypotheses for the growth mechanism were put forward.

Many studies have compared dike and fissure swarms, suggesting or refuting strong links between faults and fissures at the surface of active zones and deep dyke swarms (Helgason and Zentilli, 1985; Forslund and Guðmundsson, 1991; Guðmundsson, 1995a, b, 2003; Tentler, 2005; Paquet et al, 2007). Some authors (e.g., Rowland et al., 2007, in the Afar rift) assume (i) that normal faults are initiated or reactivated ahead of and above propagating dyke and (ii) that preexisting subvertical cooling joints are reactivated as opening mode fissures above the upper tip line of the normal faults. In such case the horizontal segmentation of the main fault traces observed every 500-1500 m in our study (Fig. 10) could have originated either via irregularities in the shape of the dike or via a segmentation of the dike itself, which is a common feature in dike patterns (e.g., Guðmundsson, 2002). However, other authors, based on field comparisons between dyke swarms and fault patterns in the eroded palaeo-rift zones, demonstrated that the number of dykes by far exceeds the number of normal faults in the same sections and even that where the dyke frequency was high, the fault frequency was low (e.g., Forslund and Guðmundsson, 1991; Guðmundsson, 2003; Paquet et al., 2007).

5.2 Segmentation and changes in the throw and length of the fault traces

Cowie and Roberts' (2001) conceptual model of fault growth shows how a set of faults connected at their tips evolves into a single fracture. Applied to the longitudinal profiles shown in Figure 10, this model can be used to interpret the different stages we observed. Cowie and Roberts distinguish two main stages (Fig. 14) in the growth of faults: a first stage of isolated growth during which the throw increases moderately compared to the length, followed by a second stage, when the segments are connected, during which there is a large increase in the throw but only a small (or no) increase in length.

Cowie and Roberts (2001) identified two ways in which this second stage can proceed, depending on whether or not the faults are strongly interconnected. When the links between the faults are weak, the junctions between the segments become complete at the end of the process, after the central parts have stopped growing. When the links between the faults are strong, the throw gradually increases everywhere and the distinctions between the segments gradually disappear. Our data show situations that may indicate a third, intermediate way for this stage to proceed (Fig. 14). Once the segments are connected, we observed an initial step (P1) during which the throw increases more in the central part of the segments than at the junctions, where the throw remains small. This is followed by a second step (P2) during which the throw differences at the junctions disappear.

Considered as a whole, R48 (Fig. 10) is an example of a fault at the end of stage 1 (Fig. 14), at which point the three segments are connected. In the following step, the throw of the central segment should increase more than the throw in the other two segments. Finally, the differences in the throws of the segments should decrease until the fault achieves an elliptical profile encompassing the three segments.

Analysis of the individual segments of faults R28 and R48 (Fig. 10) suggests that the process is more advanced than in the case of fault R48 taken as a whole. For all the segments, the throw differences at the tips of the initial segments are being reduced and the general profile is elliptical. It should be noted that the initial segments of fault R48 are ~250 m long, whereas the typical length of the segments of R28 is 500 m.

According to the conceptual model, fault R16 corresponds to the final stage in the process, when any individual segments that existed at the beginning of fault development have become indistinguishable.

5.3 Limitation of the throw and maximum throw/length ratio

The throws we measured in the VFS are significantly smaller than the throws measured in other Icelandic fissure swarms in lava flows of comparable age (Opheim and Guðmundsson, 1989; Dauteuil et al. 2001; Tentler and Mazzoli, 2005, Sonnette et al., 2010). In addition, maximum throws in the VFS are very similar between the different faults, often ~10 m. In other areas, maximum throws have been found to be related to the length of the faults by a power law (Sonnette et al., 2010).

Compared with previously published data (Gupta and Scholz, 2000), the maximum throw/fault-length ratio is small. Considering the 2-km segments along fault R48 to be single faults gives a maximum throw/fault-length ratio of 0.005, which is four times smaller than the mean ratio reported by Gupta and Scholz (2000). Consequently, the throws of the segments we measured are likely to increase without the segments necessarily increasing in length.

5.4 Interaction and linkage of fissures and normal faults

As mentioned in section 4.7, interaction and linkage zones occur in all Icelandic fissure swarms. Linkage zones have been described in similar basaltic rocks in other geodynamic contexts, such as Kilauea Volcano in Hawaii (Peacock and Parfitt, 2002; Martell and Langley, 2006), as well as in many other geological settings and rock types, especially since the early 1990s (e.g., Morley et al., 1990; dePolo et al., 1991; Peacock and Sanderson, 1991; Anders and Schlische, 1994; Gupta and Scholz, 2000; Marchal et al., 2003).

In the case of the VFS, most of the links between faults are marked by an overlap zone, with direct connections between segments occurring in only a few cases of closely aligned segments (e.g., Fig. 12b). As described in section 4.7, most of the VFS links are of immature type (connection not complete at the surface). Detailed examination of the topology of overlapping areas reveals a predominance of left stepping *en-echelon* ruptures. This may indicate a small strike-slip component in addition to the main normal movement, which is consistent with the general behavior of the area as a large, left-lateral shear zone, either partitioned into NE-SW *en-echelon* fracture zones (Clifton et al., 2003), or resembling a transtensional segmented transform, as suggested by Geoffroy et al. (2008).

5.5 Spacing of main composite fractures and thickness of layers

It should be noted that the general structure of the VFS is not that of a typical graben. The structure is not axially symmetrical, as the front of the faults in the southeast is not opposite the front of the faults in the northwest, except in the case of fault R16 (Fig. 2 and 9). The cross-sections (Fig. 9) show four or five major faults, and the boundary and central faults have similar throws. The spacing of parallel main composite fractures contains at least two modes at 225 m and 450 m (Fig. 8). It should be noted that spacing of large fault zones in Holocene Icelandic fissure swarms is very variable (e.g., Guðmundsson, 1987a,b; Opheim and Guðmundsson, 1989), suggesting that the fault spacing may change during the lifetime of a fissure swarm (Forslund and Guðmundsson, 1991).

The relationship between the spacing of the fracture zones and the thickness of the brittle behavior levels has already been noted (e.g., Bai and Pollard, 2000; Ackermann et al., 2001). Seismicity in our study area appears to be restricted to depths of less than 7-8 km, with most earthquakes occurring at 4-6 km (Keiding et al., 2008). These values are too high to be related directly to the observed spacing; however, they are similar to the total width of the fissure swarm.

Grant and Kattenhorn (2004) modeled normal faulting ending at depths of 250 and 500 m, and extending to the surface along vertical fractures. They interpreted these structures as ancient faults affecting deep layers that have subsequently been covered by younger lava flows. Reactivation of these faults could lead to the development of vertical extensions. Grant and Kattenhorn noted the presence of major discontinuities at depths of 250 and 500 m, which could be the cause of mechanical decoupling. Another possibility, related to the potential control of the geometry and development of the fault patterns by dykes is that the spacing of the major fault zones reflects the spacing between the underlying dikes. This is however unlikely in so far as some field studies (see section 5.1) have demonstrated that there is no systematic relationship between fault and dyke swarms. Finally, it is also possible that the different modes corresponds to different causes, including a mechanical decoupling and also possibly reflecting the intrinsic mechanical properties of the upper levels of the brittle crust.

6. Conclusion

(1) Advanced photogrammetric techniques allowed us to accurately map the VFS and differentiate between fissures and faults. We measured the throws of vertical faults with throws greater than 0.5 m along five of the main fracture zones. By using remote sensing methods we were able to carry out a comprehensive study of the area much more quickly than would have been possible if we had relied solely on field measurements.

(2) The fracturing of the VFS includes both fissures (without vertical throw) and normal faults (with vertical throw), both of which are generally accompanied by opening (from several millimeters to several meters). Most of the fractures are grouped together into main composite lines that generally include both fissures and normal faults. Seven of the normal fault lines are longer than 2500 m. They mostly correspond to the main fault scarps of the fissure swarm. The maximum throw is ~10 m and seems to be independent of the total length of the fault.

(3) The VFS is an uncommon graben-like structure, bounded to the east and to the west by major normal faults that face west and east, respectively. Faulting deformation between the two boundary faults is mostly accommodated by regularly spaced, west-dipping normal faults. The throws of the boundary and inner faults are not significantly different.

(4) The structure of the fault zone may be closely linked to the network of underlying dikes. When stopped in their progression toward the surface, these dikes may extend upwards as normal faults, which will therefore show similar spacing to the dikes.

(5) In the throw profiles along the fully visible major normal faults, throws are biggest in the central part of the fault segments and decrease towards the segment tips. Composite faults contain several segments. The boundaries between the different segments remain visible for almost the whole growth period.

(6) Detailed analysis of the throw profiles revealed different steps in the fault growth process. The first step is characterized by a moderate increase in throw compared to the increase in length, whereas the second step involves an increase in throw with no or very little increase in length.

(7) The faults in the VFS appear to be very long compared to their throws, suggesting that they may be immature faults with a high potential for further growth. Given the current lengths of the faults, their throws could be expected to increase 3-5 fold without significant lengthening.

(8) Analysis of the linkage zones between fault segments revealed a slight but systematic shearing component. This is consistent with the general transform behavior of the Reykjanes Peninsula.

Acknowledgements

We thank Yves Egels for allowing us to use his Poivilliers software for the stereoscopic analysis. Jacques Angelier, Olivier Dauteuil and Guillaume Biessy helped with GCP acquisition. Jacques Angelier also assisted with the production of the photo-mosaics and provided encouragement during the initial stages of the study. We are grateful to Alexandre Lethiers (ISTeP) and André Paillet (Edytem) for their help in drawing the figures. We thank Paul Henderson who read the manuscript and significantly improved our English writing. Águst Guðmundsson and Valerio Acocella are thanked for their helpful reviews and comments. Financial support was provided by the French Polar Institute (IPEV) via Arctic Program 316 IPCROCI.

References

Ackermann, R.W., Schlische, R.W., Withjack, M.O., 2001. The geometric and statistical evolution of normal fault systems: an experimental study of the effects of mechanical layer thickness on scaling laws. Journal of Structural Geology 23, 1803-1819.

Acocella, V., Guðmundsson, Á., Funiciello, R., 2000. Interaction and linkage of extension fractures and normal faults: examples from the rift zone of Iceland. Journal of Structural Geology 22, 1233-1246.

Acocella, V., Korme, T., Salvini, F., 2003. Formation of normal faults along the axial zone of the Ethiopian Rift. Journal of Structural Geology 25, 503-513.

Anders, M.H., Schlische, R.W., 1994. Overlapping faults, intra-basin highs, and the growth of normal faults. Journal of Geology 102, 165-180.

Angelier, J., Bergerat, F., Dauteuil, O., Villemin, T., 1997. Effective tension-shear relationships in extensional fissure swarms, axial rift zone of northeastern Iceland. Journal of Structural Geology 19, 673-685.

Árnadóttir, Th., Geirsson, H., Jiang, W., 2008. Crustal deformation in Iceland: Plate spreading and earthquake deformation. Jökull 58, 59-74.

Bai, T., Pollard, D.D., 2000. Fracture spacing in layered rocks: a new explanation based on the stress transition. Journal of Structural Geology 22, 43-57.

Cartwright, J.A., Trudgill, B.D., Mansfield, C.S., 1995. Fault growth by segment linkage: an explanation for scatter in maximum displacement and trace length data from the Canyonlands Grabens of SE Utah. Journal of Structural Geology 17, 1319-1326.

Childs, C., Watterson, J., Walsh, J.J., 1995. Fault overlap zones within developing normal fault systems. Journal Geological Society London 152, 535-549.

Childs, C., Nicol, A., Walsh, J.J., Watterson, J., 1996. Growth of vertically segmented normal faults. Journal of Structural Geology 18, 1389-1397.

Clifton, A.E., Kattenhorn, S.A., 2006. Structural architecture of a highly oblique divergent plate boundary segment. Tectonophysics 419, 27-40.

Clifton, A.E., Pagli, C., Jónsdóttir, J.F., Eythorsdóttir, K., Vogfjörð, K., 2003. Surface effects of triggered fault slip on Reykjanes Peninsula, SW Iceland. Tectonophysics 369, 145-154.

Cowie, P.A., Knipe, R.J., Main, I.G., 1996. Introduction to the special issue: Scaling laws for fault and fracture populations, analyses and applications. Journal of Structural Geology 18, v-xi.

Cowie, P.A., Roberts, G.P., 2001. Constraining slip rates and spacings for active normal faults. Journal of Structural Geology 23, 1901-1915.

Dauteuil, O., Angelier, J., Bergerat, F., Verrier, S., Villemin, T., 2001. Deformation partitioning inside a fissure swarm of the northern Icelandic rift. Journal of Structural Geology 23, 1359-1372.

dePolo, C.M., Clark, G.C., Slemmons, D.B., Ramelli, A.R., 1991. Historical surface faulting in the Basin and Range province, western North America: implications for fault segmentation. Journal of Structural Geology 13, 123-136.

DeMets, C., Gordon, R.G., Argus, F., Stein, S., 1990. Current plate motions. Geophysical Journal International 101, 425-478.

DeMets, C., Gordon, R.G., Argus, F., Stein, S., 1994. Effect of recent revisions to the geomagnetic reversal time scale on estimates of current plate motions. Geophysical Research Letters 21, 2191-2194.

Einarsson, P., 1991. Earthquakes and present-day tectonism in Iceland. Tectonophysics 189, 261-279.

Forslund, T., Guðmundsson, A., 1991. Crustal spreading due to dikes and faults in southwest Iceland. Journal of Structural Geology 13, 443-457.

Friese, N., 2008. Brittle tectonics of the Thingvellir and Hengill volcanic systems, Southwest Iceland: field studies and numerical modelling. Geodinamica Acta 21, 169-185.

Geoffroy, L., Dorbath, C., 2008. Deep downward fluid percolation driven by localized crust dilatation in Iceland. Geophysical Research Letters 35, L17302, doi:10.1029/2008GL034514.

Grant, J.V., Kattenhorn, S.A., 2004. Evolution of vertical faults at an extensional plate boundary, Southwest Iceland. Journal of Structural Geology 26, 537-557.

Guðmundsson, Á., 1980. The Vogar fissure swarm, Reykjanes peninsula, SW Iceland. Jökull 30, 43-64.

Guðmundsson Á., 1986. Mechanical Aspects of Postglacial Volcanism and Tectonics of the Reykjanes Peninsula, Southwest Iceland. Journal of Geophysical Research 91, 12711-12721

Guðmundsson, Á., 1987a. Geometry, formation and development of tectonic fractures on the Reykjanes Peninsula, Southwest Iceland. Tectonophysics 139, 295-308.

Guðmundsson, Á., 1987b. Tectonics of the Thingvellir Fissure Swarm, SW Iceland. Journal of Structural Geology 9, 61-69.

Guðmundsson, Á., 1992. Formation and growth of normal faults at the divergent plate boundary in Iceland. Terra Nova 4, 464-471.

Guðmundsson, Á., 1995a. The geometry and growth of dikes. In: Baer, G., Heimann, A. (Eds.), Physics and Chemistry of Dikes. Balkema, Rotterdam, 23–34.

Guðmundsson, Á., 1995b. Infrastructure and mechanisms of volcanic systems in Iceland. Journal of Volcanology and Geothermal Research 64, 1-22

Guðmundsson, Á., 2002. Emplacement and arrest of sheets and dikes in central volcanoes. Journal of Volcanology and Geothermal Research, 116, 279-298.

Guðmundsson, Á., 2003. Surface stresses associated with arrested dykes in rift zones. Bulletin of Volcanology 65, 606-618.

Guðmundsson, Á., 2011. Rock fractures in geological processes. Cambridge University Press, 578 p.

Guðmundsson, Á., Bäckström K., 1991. Structure and development of the Sveinagjá graben, Northeast Iceland. Tectonophysics 200, 111-125.

Gupta, A., Scholz, C.H., 2000. A model of normal fault interaction based on observations and theory . Journal of Structural Geology 22, 865-879.

Haimson , B.C., Rummel, F., 1982. Hydrofracturing stress measurements in the Iceland research drilling project drill hole at Reyðarfjörður, Iceland. Journal of Geophysical Research 87, 6631-6649.

Helgason, J., Zentilli, M., 1985. Field characteristics of laterally emplaced dikes: anatomy of an exhumed Miocene dike swarm in Reydarfjördur, eastern Iceland. Tectonophysics 115, 247-274.

Hjartardóttir, Á. R., Einarsson, P., Sigurdsson, H., 2009. The fissure swarm of the Askja volcanic system along the divergent plate boundary of N Iceland. Bulletin Volcanology 71, 961-975.

Hreinsdóttir, S., Einarsson, P., Sigmundsson, F., 2001. Crustal deformation at the oblique spreading Reykjanes Peninsula, SW Iceland: GPS measurements from 1993 to 1998. Journal of Geophysical Research 106, 13803-13816.

Huggins, P., Watterson, J., Walsh, J.J., Childs, C., 1995. Relay zone geometry and displacement transfer between normal faults recorded in coal-mine plans. Journal of Structural Geology 17, 1741-1755.

Jóhannesson, H., Sæmundsson, K., 2009. Geological map of Iceland, Bedrock Geology. Icelandic Institute of Natural History, Reykjavik , 1st ed., scale 1:600 000.

Kasser, M., Egels, Y., 2001. Digital photogrammetry. Taylor and Francis, London.

Keiding, M., Árnadóttir, T., Sturkell, E., Geirsson, H., Lund, B., 2008. Strain accumulation along an oblique plate boundary: The Reykjanes Peninsula, southwest Iceland, Geophysical Journal International 172, 861 – 872, doi:10.1111/j.1365–246X.2007.03655.x.

Keiding, M., Lund, B., Árnadóttir, T., 2009. Earthquakes, stress and strain along an obliquely divergent plate boundary: the Reykjanes Peninsula, southwest Iceland, Journal of Geophysical Research 114, 861-872, B09306, doi: 10.1029/2008JB006253.

Mansfield, C. S., Cartwright, J. A., 1996. High resolution fault displacement mapping from three-dimensional seismic data: evidence for dip linkage during fault growth. Journal of Structural Geology 18, 249-263.

Marchal, D., Guiraud, M., Rives, T., 2003. Geometric and morphologic evolution of normal fault planes and traces from 2-D to 4-D data. Journal of Structural Geology 25, 135-158.

Martel, S.J., Langley, J.S., 2006. Propagation of normal faults to the surface in basalt, Koae fault system, Hawaii. Journal of Structural Geology 28, 2123-2143.

Morley, C.K., Nelson, R.A., Patton, T.L., Munn, S.G., 1990. Transfer zones in the East African rift system and their relevance to hydrocarbon exploration in rifts. Bulletin American Association Petroleum Geology 74, 1234-1253.

Opheim, J. A., Guðmundsson, Á., 1989. Formation and geometry of fractures, and related volcanism, of the Krafla fissure swarm, northeast Iceland, Bulletin of the Geological Society of America, 101, 1608-1622.

Papanikolaou, I.D., Roberts, G.P., 2007. Geometry, kinematics and deformation rates along the active normal fault system in the southern Apennines: Implications for fault growth, Journal of Structural Geology 29, 166-188, doi: 10.1016/j.jsg.2006.07.009.

Paquet, F., Dauteuil, O., Hallot, E., Moreau, F., 2007. Tectonics and magma dynamics coupling in a dyke swarm of Iceland, Journal of Structural Geology 29, 1477-1493.

Peacock, D.C.P., 1991. Displacements and segment linkage in strike-slip fault zones. Journal of Structural Geology 13, 721-733.

Peacock, D.C.P., Parfitt, E.A., 2002. Active relay ramps and normal fault propagation on Kilauea Volcano, Hawaii. Journal of Structural Geology 24, 729-742.

Peacock, D.C.P., Zhang, X., 1993. Field examples and numerical modeling of oversteps and bends along normal faults in cross-section. Tectonophysics 234, 147-167.

Peacock, D.C.P., Sanderson D.J., 1991, Displacements, segment linkage and relay ramps in normal fault zones. Journal of Structural Geology 13, 721-733.

Roberts, G.P., Michetti, A.M., 2004. Spatial and temporal variations in growth rates along active normal fault systems: an example from The Lazio–Abruzzo Apennines, central Italy. Journal of Structural Geology 26, 339–376.

Rowland, J. V., Baker, E., Ebinger, C. J., Keir, D., Kidane, T., Biggs, J., Hayward, N., Wright, T. J., 2007. Fault growth at a nascent slow-spreading ridge: 2005 Dabbahu rifting episode, Afar. Geophysical Journal International 171, 3, 1226–1246.

Sæmundsson, K., 1978. Fissure swarms and central volcanoes of the neovolcanic zones in Iceland. In : Bowes, D.R., Leake, B.E. (Eds), Crustal Evolution in Northwestern Britain and Adjacent Regions. Geological Journal Special Issue 10, 415-432.

Sæmundsson, K., 1979. Outline of the geology of Iceland. Jökull 29, 7-28.

Sæmundsson, K., 1992. Geology of the Thingvallavatn area. Oikos 64, 40-68.

Scholz, C. H., 2002. The Mechanics of Earthquakes and Faulting, Cambridge Univ. Press, New York.

Schöpfer, M.P.J., Childs, C., Walsh, J.J., 2006. Localisation of normal faults in multilayer sequences. Journal of Structural Geology 28, 816-833.

Sonnette, L., Angelier, J., Villemin, T., Bergerat, F., 2010. Faulting and fissuring in active oceanic rift: Surface expression, distribution and tectonic-volcanic interaction in the Thingvellir Fissure Swarm, Iceland. Journal of Structural Geology 32, 407–422.

Tentler, T., 2005. Propagation of brittle failure triggered by magma in Iceland. Tectonophysics 406, 17-38.

Tentler, T., Mazzoli, S., 2005. Architecture of normal faults in the rift zone of central north Iceland. Journal of Structural Geology 27, 1721-1739.

Torabi, A., Berg, S.S., 2011. Scaling of fault attributes: A review. Marine and Petroleum Geology, 28, 1444-1460.

Tryggvason, E., 1974. Vertical crustal movement in Iceland. In: Kristjanson, L. (ed), Geodynamics of Iceland and the North Atlantic Area. Reidel, Dordrecht, 241-262.

Tryggvason, E., 1982. Recent ground deformation in continental and oceanic rift zones. In: Pálmason, G. (ed), Continental and Oceanic Rifts. AGU, Washington, Geodynamic Series 8, 17-29.

Figure captions

Figure 1 - The Vogar Fissure Swarm (VFS) in southwest Iceland. A: The on-land neovolcanic rift in Iceland. The main fissure swarms are shown in grey. EVZ, NVZ and WVZ are the Eastern, Northern and Western Volcanic Zones, respectively. SISZ: South Iceland Seismic Zone. TFZ: Tjörnes Fracture Zone. V: Vatnajökull; B: Location of the four main fissure swarms in the Reykjanes Peninsula, H: Hengill central volcano. C: Schematic tectonic map of the Reykjanes fissure swarm. In light grey: Upper Pleistocene basic and intermediate hyaloclastites and lavas, younger than 0.8 m.yr. In white: Postglacial basic and intermediate lavas, older than AD 871. In dark grey: Postglacial basic and intermediate lavas, younger than AD 871, main normal faults are shown as thin lines with barbs. B and C modified after Sæmundsson (1979), Sæmundsson and Einarsson (1980), Guðmundsson (1986, 1987a), and Jóhannesson and Sæmundsson (2009).

Figure 2 - Aerial photograph mosaic of the VFS (photographs O8750, O8751 and O8752, 1998, from "Landmælingar Íslands"). All fractures identified in this study are shown as colored lines: East dipping normal faults in blue, with important opening shown in black; west dipping normal faults in green, with important opening shown in yellow; fissures (pure tension fracture) without vertical throw (or vertical throw smaller than 0.5 m) in red. Most of these fractures are concentrated within several fracture zones shown in Figure 3. Location grid uses UTM coordinates.

Figure 3 - Main composite fractures of the VFS and location of the along-strike and across-strike profiles. The thick grey lines are the main composite fractures; the black lines are fractures for which we plotted along-strike profiles. Numbers (R) refer to the main composite fractures described in the text. Small arrows numbered 0 to 70 indicate the locations of the across-strike profiles. Blue bands indicate the across-strike profiles shown in Figure 9. The red rectangle shows the location of Figure 11. Rose diagrams show the trends of the 156 individual faults and 322 individual fissures.

Figure 4 - West-facing, sub-parallel normal fault scarps illustrating the step pattern in the VFS. A: Oblique aerial photograph taken from a helicopter (looking east), B: Detail of two steps (looking southeast).

Figure 5 - A west-facing normal fault with opening in the VFS. The vertical throw is ~2 m. Note the graben-like structure characteristic of near-surface normal faulting (i.e., fault with both vertical and opening components).

Figure 6 - Fissures in the VFS. A: aerial photograph of a long fissure, taken from a helicopter (looking northeast), B: fissure with a small vertical throw (smaller than 0.5 m) observable near the photographer, C: detail of a small fissure opening; part of the fissure follows the columnar joints yielding zigzag geometry.

Figure 7 - Distribution of fracture lengths. Histograms showing the number of fractures (N) as a function of fracture length (L, in meters), with classes of 25 m for individual fissures (A) and individual faults (B), and with classes of 250 m for main composite fractures (C).

Figure 8 – Spacing of fractures in the VFS, with number of fractures (N) plotted as a function of spacing (S, in meters). In blue (lozenges): All individual fractures (fissures and faults). In red (squares): Individual fissures. In green (triangles): Main composite faults.

Figure 9 – Changes in the topography across the VFS. Sections 23-27 and 50-54 as examples (see location in Figure 3). The number of main composite fractures cut by the profiles is indicated. Lengths and altitudes are in meters. A-D profiles are enlargements of fault scarps R16 and R28, which face east and west, respectively.

Figure 10 – Along-strike changes in fault throw for main composite fractures R16, R24 R28, R38 and R48 (see location in Figure 3). All throws and distances are in meters. Throw profile established from the along-strike topographic profiles at a distance of 20 m from the main discontinuity are shown as black lines, and at a distance of 40 m are shown as grey lines.

Figure 11 - Detailed view of the central part of fracture R38 and its junction with fracture R36 (mosaic of a dozen oblique aerial photographs taken from a helicopter). Note the smaller shadow of fault R38 in the left-hand two thirds of the mosaic, indicating a decrease in its throw (here, the deformation is accommodated by R38 and by R36, which are parallel, see location in Figure 3).

Figure 12 – Fault tips and fault linkages at the surface (aerial photographs taken from a helicopter). (a) Non-overlapping close segments. (b) Non-overlapping segments with oblique fracture forming the junction. (c) Poorly overlapping segments with each tip propagating to the sidewall of the other segment. (d) Horsetail-type tip of a fault segment in the linkage zone with another segment. (e) Amply overlapping sub-parallel close segments. (f) Non-overlapping segment with sub-parallel en-echelon fractures forming the junction. (g) Complex linkage zone including oblique and sub-parallel fractures. (h) Detail of the horsetail tip of a fault.

Figure 13 – Immature and mature junctions between fault traces. It is possible to pass from one side to the other of an immature fault without crossing any fractures (as shown by the dotted line). In the mature state, the two fault segments are connected and the two sides of the fault are fully separated.

Figure 14 – Conceptual model of fault growth in the VFS (adapted from Cowie and Roberts, 2001; Roberts and Michetti, 2004; Papanikolaou and Roberts, 2007). (a) Model of throw-fault length profile. Fault segments initially grow by increasing in length and in throw (stage 1). At the end of stage 1, fault linkage occurs and fault segments interact over long distances (stage 2). (b) Graph showing throw as a function of time for the central segment shown in (a). This illustrates the throw enhancement rate as interaction and linkage proceed. See text for a detailed explanation. SB: Segment boundary, d1: Maximum throw on each segment prior to linkage, d2: Maximum throw on the entire fault after linkage, L1: Length of a single segment, L2: Length of the fault after linkage.

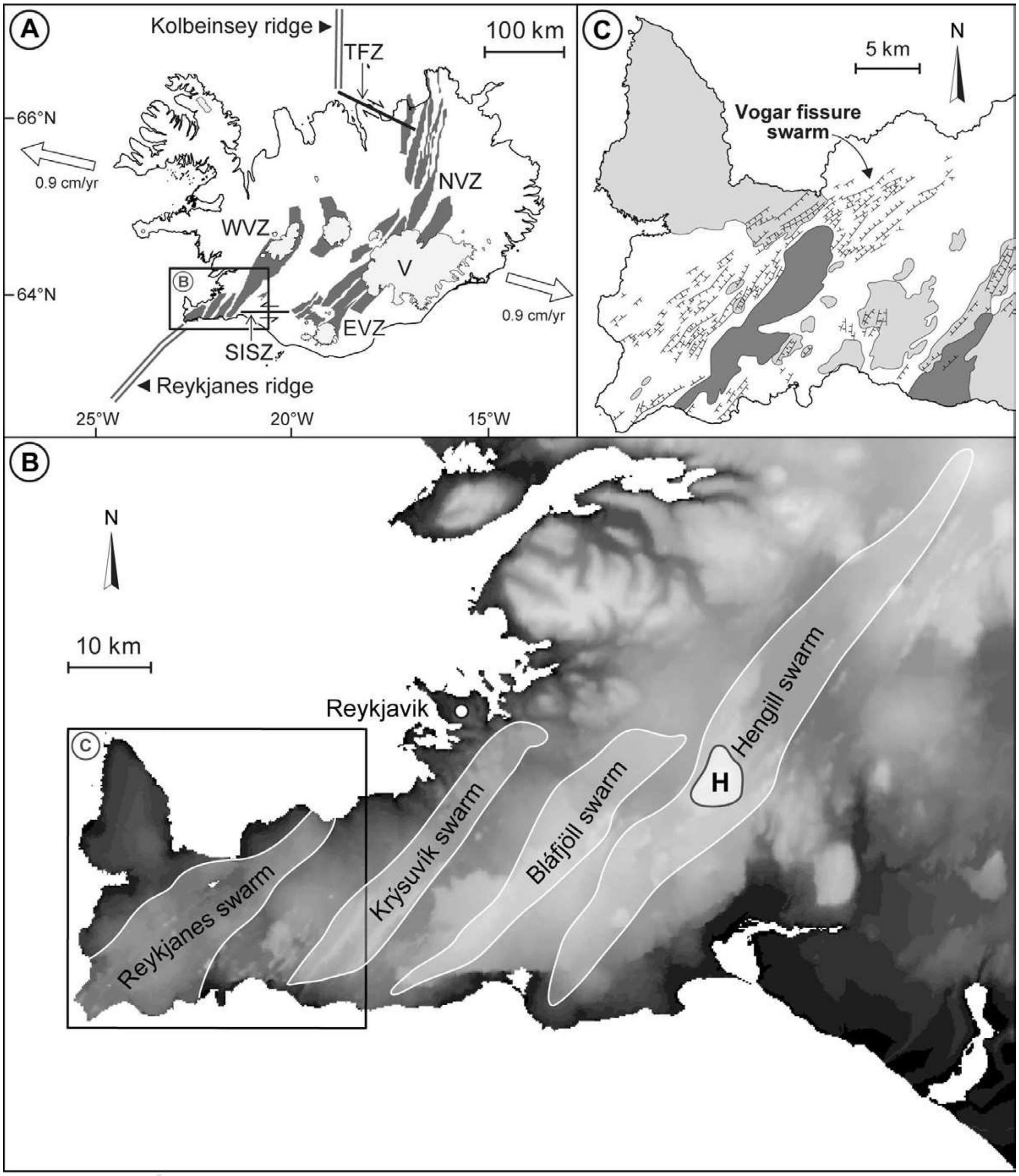
A
Kolbeinsey ridge
TFZ
100 km
66°N
0.9 cm/yr
NVZ
WVZ
V
B
64°N
EVZ
0.9 cm/yr
SISZ
Reykjanes ridge
25°W
20°W
15°W
C
5 km
N
Vogar fissure swarm
B
N
10 km
Reykjavik
C
Hengill swarm
H
Krýsuvík swarm
Bláfjöll swarm
Reykjanes swarm

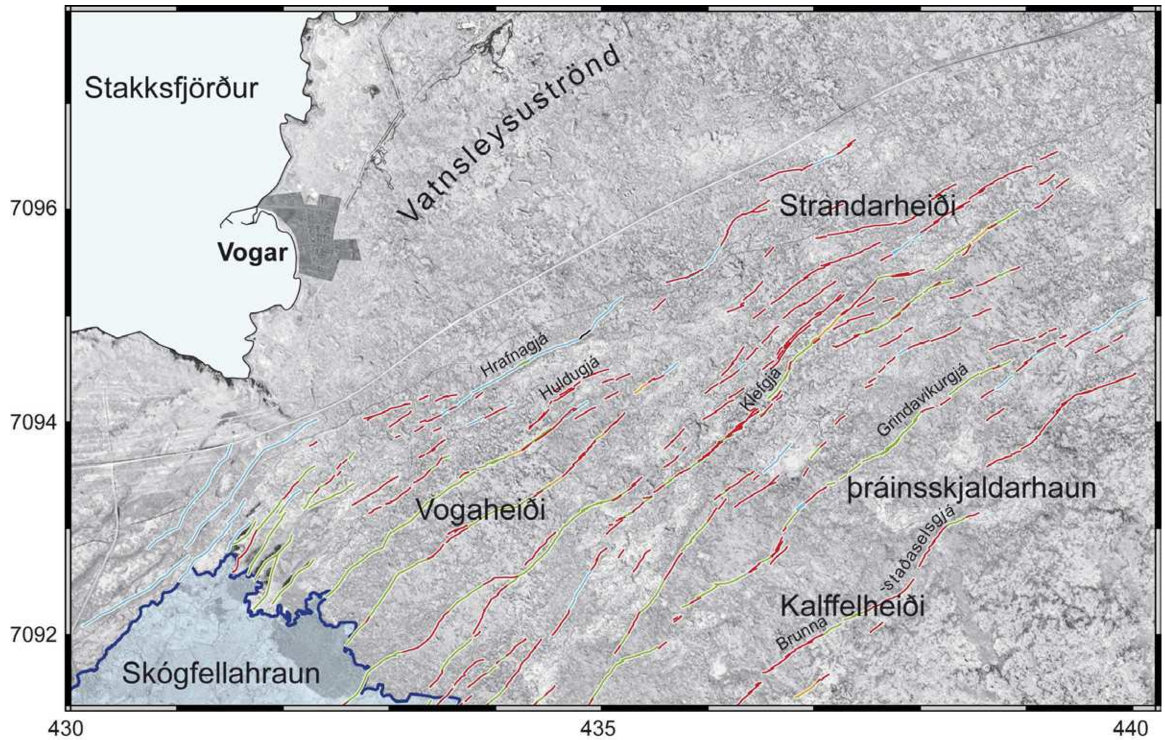
Stakksfjörður
Vatnsleysuströnd
Vogar
Strandarheiði
Hrafnagjá
Huldugjá
Klefgjá
Grindavíkurgjá
Vogaheiði
þráinsskjaldarhaun
Staðaselsgjá
Kalffelheiði
Brunna
Skógfellahraun
7096
7094
7092
430
435
440

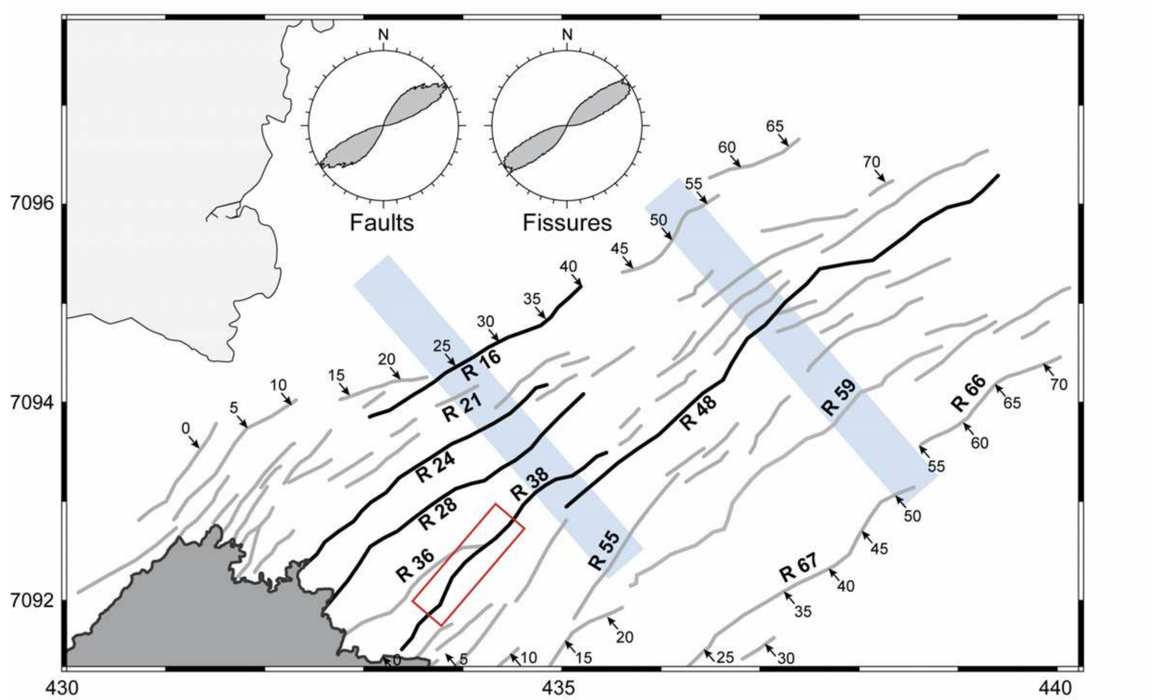

N
Faults
Fissures
7096
7094
7092
430
435
440
R 16
R 21
R 24
R 28
R 36
R 38
R 55
R 48
R 59
R 66
R 67


A
B


A
B
C

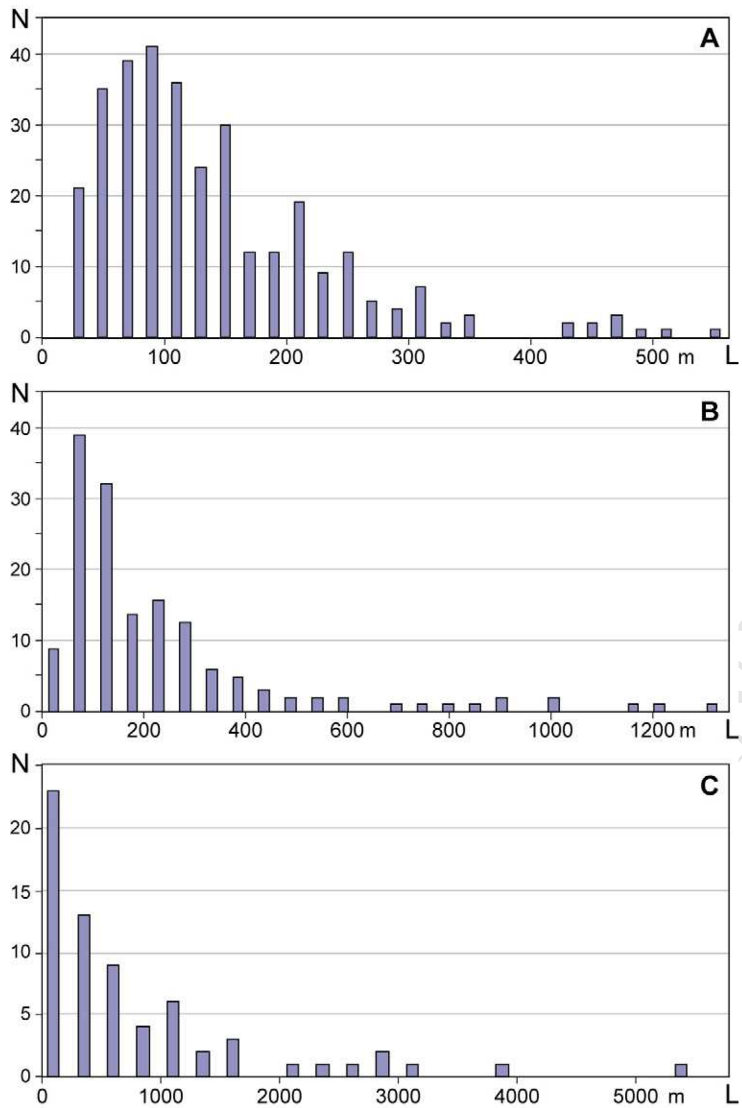
N
A
40
30
20
10
0
0
100
200
300
400
500 m
L
N
B
40
30
20
10
0
0
200
400
600
800
1000
1200 m
L
N
C
20
15
10
5
0
0
1000
2000
3000
4000
5000 m
L

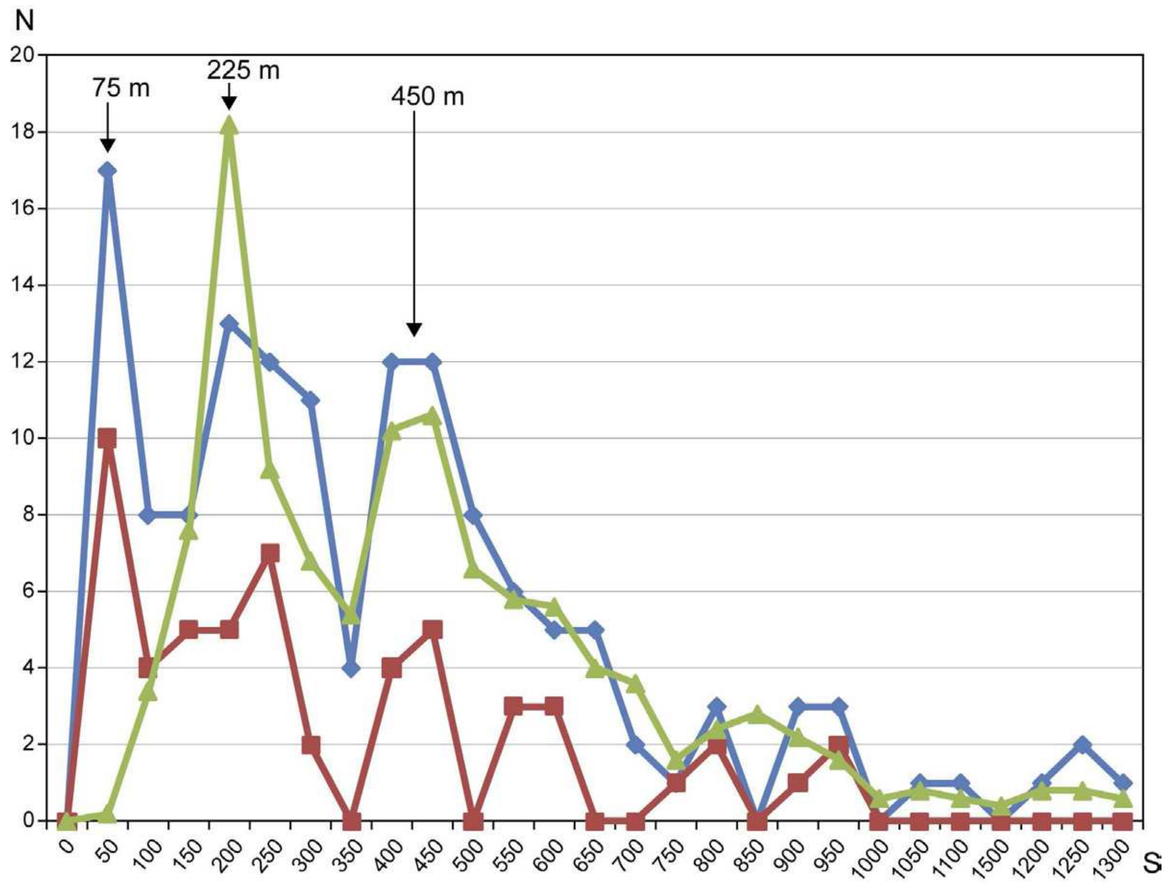
N
20
18
16
14
12
10
8
6
4
2
0
75 m
225 m
450 m
0
50
100
150
200
250
300
350
400
450
500
550
600
650
700
750
800
850
900
950
1000
1050
1100
1500
1200
1250
1300
S

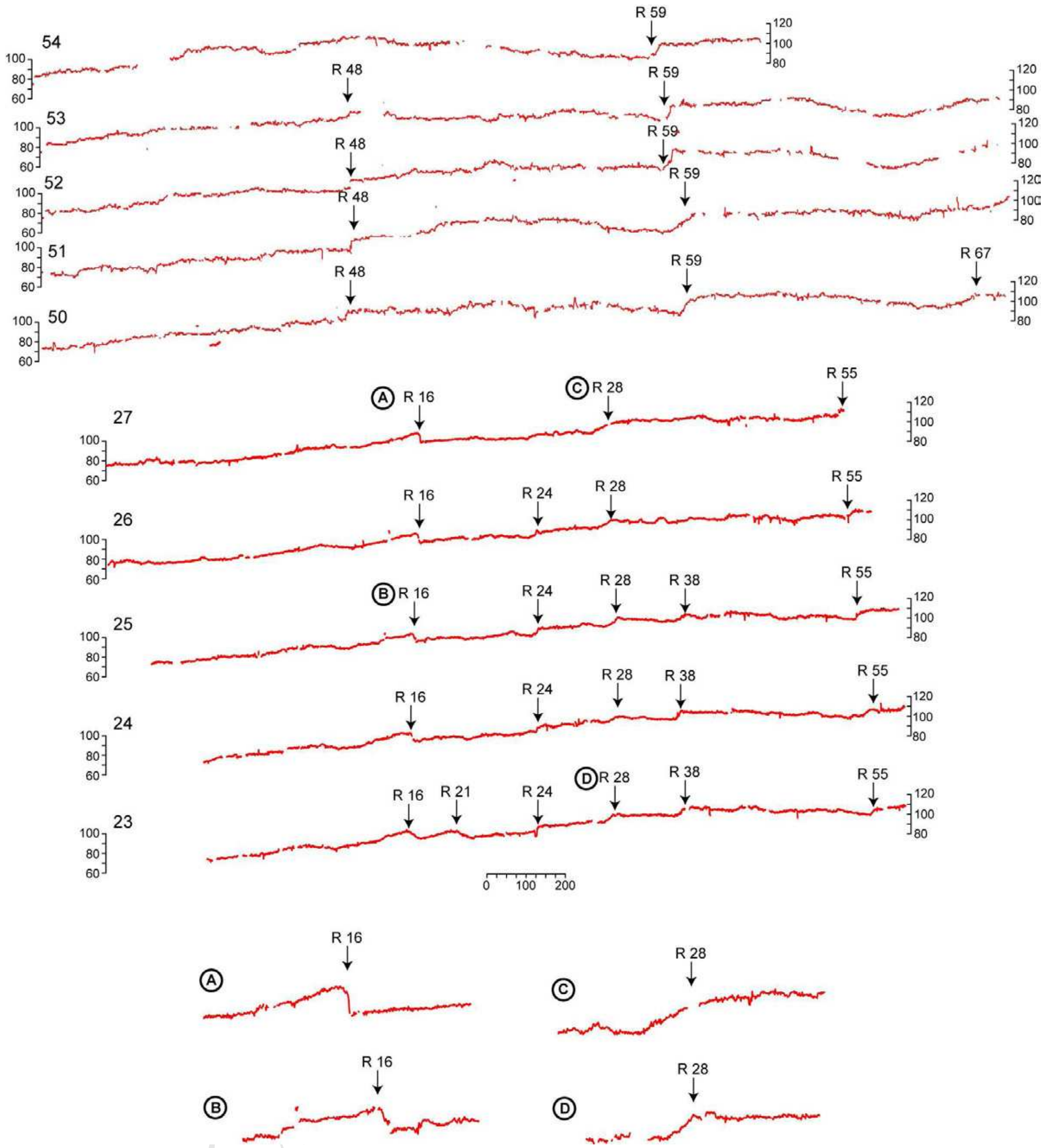

54
53
52
51
50
R 48
R 59
R 67
27
26
25
24
23
R 16
R 21
R 24
R 28
R 38
R 55
A
B
C
D
0
100
200

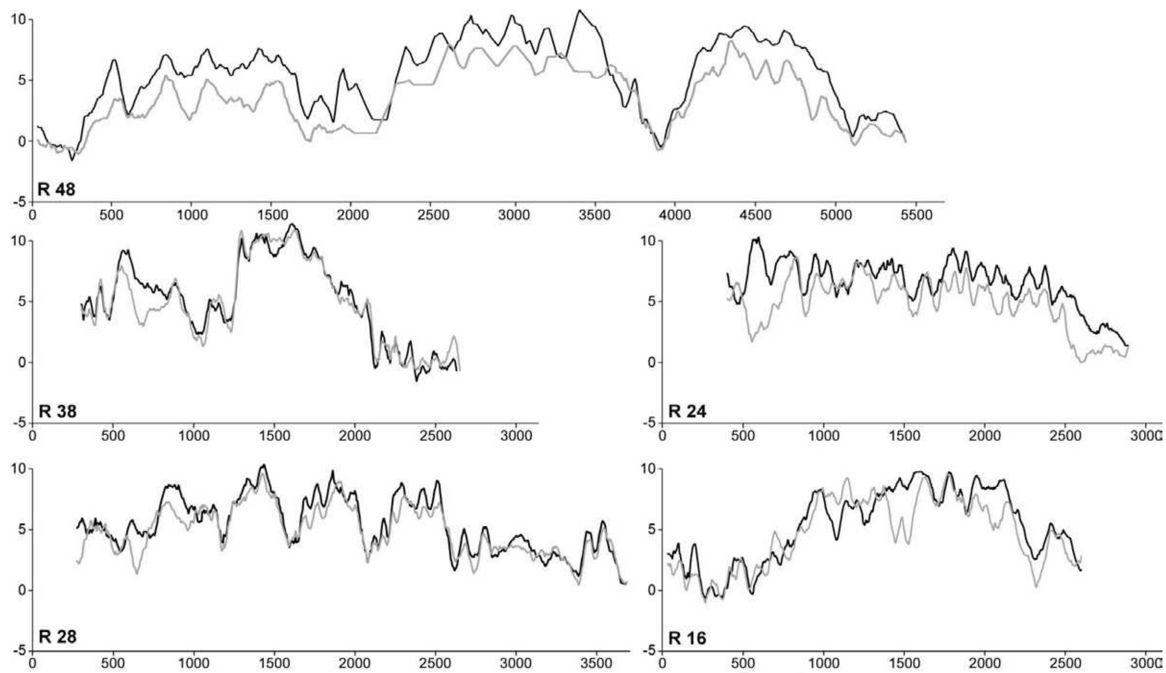
R 48
R 38
R 24
R 28
R 16

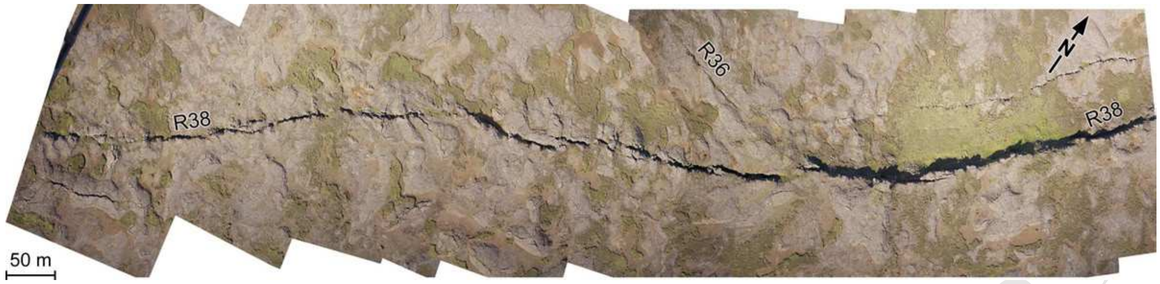
R38
R36
R38
N
50 m

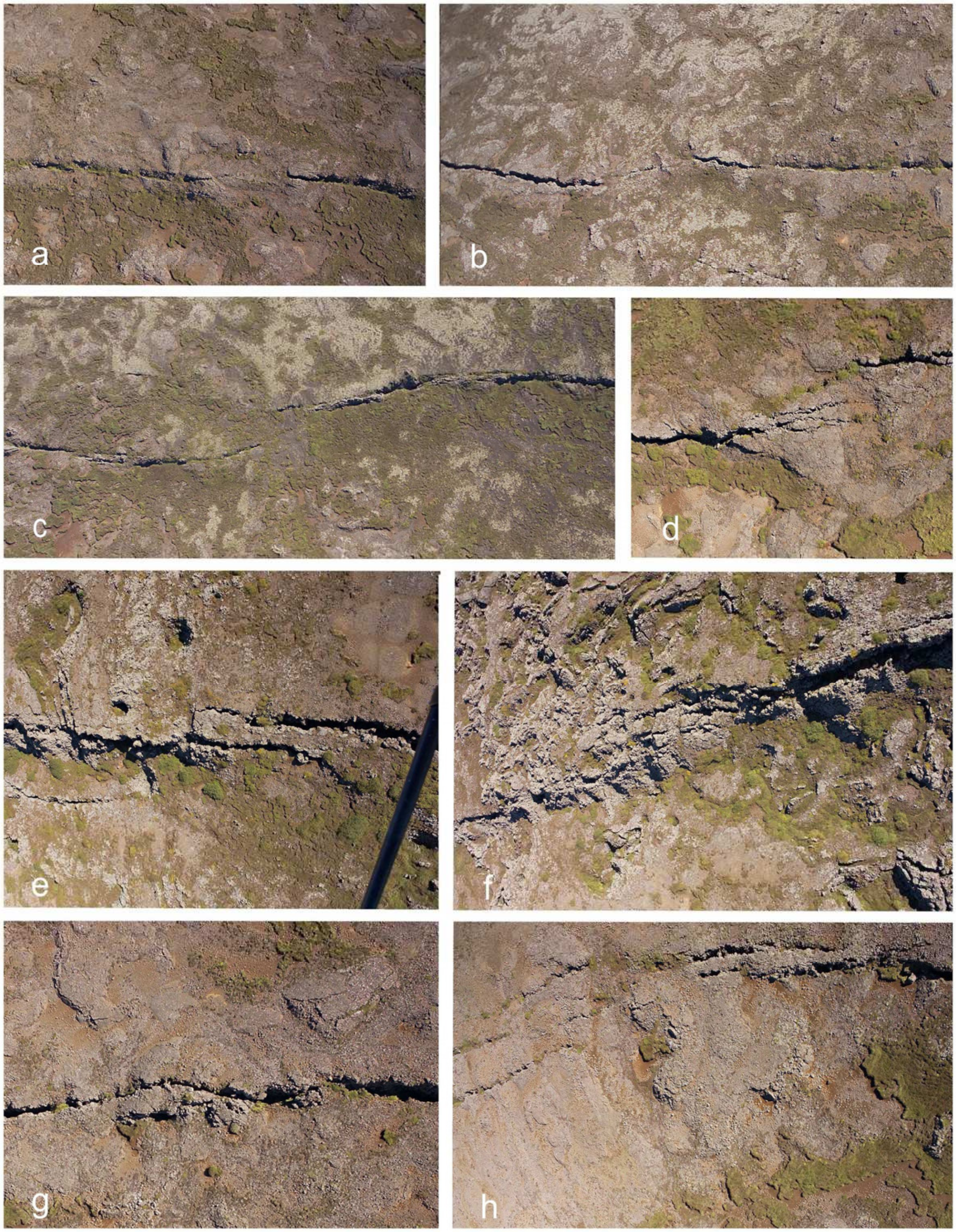
a
b
c
d
e
f
g
h

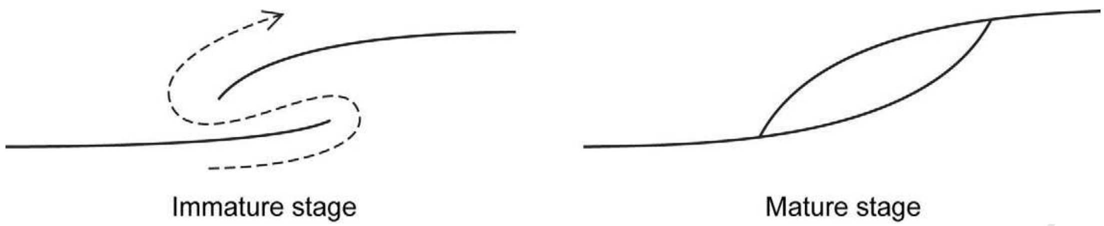
Immature stage
Mature stage

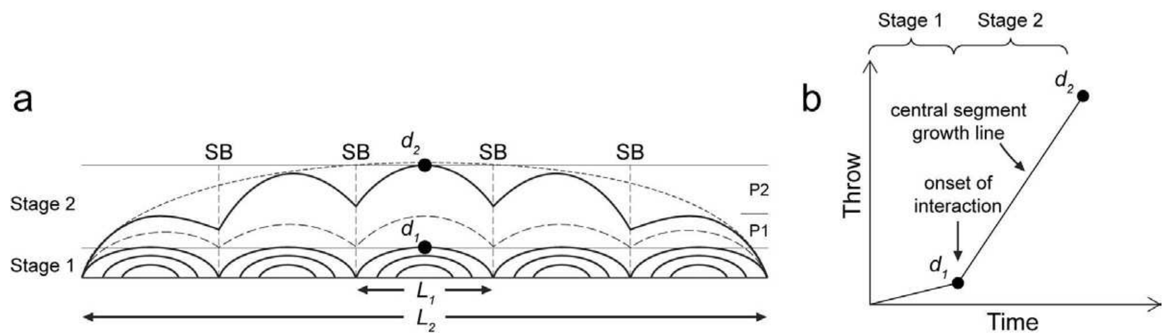
a
SB
SB
SB
SB
d2
d1
Stage 2
Stage 1
P2
P1
L1
L2
b
Stage 1
Stage 2
d2
central segment
growth line
onset of
interaction
d1
Throw
Time